New Insights on the Molecular Mechanism for the Recalcitrance of Biochars: Interactive Effects of Carbon and Silicon Components.

Article *in* Environmental Science and Technology · July 2014

DOI: 10.1021/es405647e · Source: PubMed

2 authors:

Guo Jianhua
Hebei University of Engineering
5 PUBLICATIONS **209** CITATIONS

SEE PROFILE

Baoliang Chen
Zhejiang University
198 PUBLICATIONS **16,102** CITATIONS

SEE PROFILE

Environmental Science & Technology

Article

pubs.acs.org/est

Insights on the Molecular Mechanism for the Recalcitrance of Biochars: Interactive Effects of Carbon and Silicon Components

Jianhua Guo[†,‡] and Baoliang Chen*[,†,‡]

[†]Department of Environmental Science, Zhejiang University, Hangzhou 310058, China

[‡]Zhejiang Provincial Key Laboratory of Organic Pollution Process and Control, Hangzhou 310058, China

Supporting Information

ABSTRACT: Few studies have investigated the effects of structural heterogeneity (particularly the interactions of silicon and carbon) on the mechanisms for the recalcitrance of biochar. In this study, the molecular mechanisms for the recalcitrance of biochars derived from rice straw at 300, 500, and 700 °C (named RS300, RS500, and RS700, respectively) were elucidated. Short-term (24 h) and long-term (240 h) oxidation kinetics experiments were conducted under different concentrations of H_2O_2 to distinguish the stable carbon pools in the biochars. We discovered that the stabilities of the biochars were influenced not only by their aromaticity but also through possible protection by silicon encapsulation, which is regulated by pyrolysis temperatures. The aromatic components and recalcitrance of the biochars increased with increasing pyrolysis temperatures. The morphologies of the carbon forms in all of the biochars were also greatly associated with those of silica. Silica-encapsulation protection only occurred for RS500, not for RS300 and RS700. In RS300, carbon and silica were both amorphous, and they were easily decomposed by H_2O_2. The separation of crystalline silica from condensed aromatic carbon in RS700 eliminated the protective role of silicon on carbon. The effect of the biochar particle size on the stability of the biochar was greatly influenced by C−Si interactions and by the oxidation intensities. A novel silicon-and-carbon-coupled framework model was proposed to guide biochar carbon sequestration.

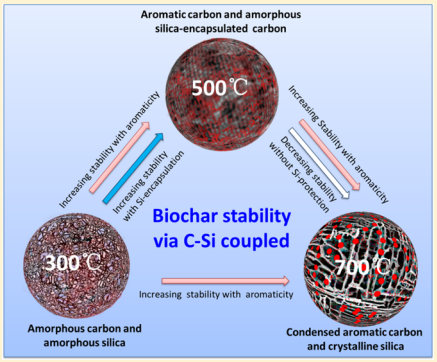

INTRODUCTION

Biochar is a carbon-rich residue that is formed during the pyrolysis of biomass, and it has been shown to be highly stable, persisting longer in soils than other forms of soil organic matter.[1,2] Therefore, biochar amendment is considered to be an emerging tool for carbon sequestration.[3] Biochar is characterized as a heterogeneous material with a range of partially to completely carbonized carbon forms,[4−7] and it contains different forms of crystallized aromatic carbons and non-polyaromatic carbons,[8,9] as well as distinct ash contents in biochars derived from various feedstocks.[10,11] Aromatic carbon typically has the greatest contribution to the recalcitrance of biochar.[2] Understanding the long-term stability of biochar is hindered by its heterogeneous nature and particulate form.[2,12,13] The oxidation of biochar typically begins on its surfaces. Therefore, quantifying the decomposition of fresh biochar may lead to an overestimation of its long-term decay.[2,9] A recent report revealed that CO_2 production primarily originated from polycyclic aromatic components rather than from any minor labile components for biochars that were produced at 650 and 700 °C by short-term lab incubation and with a predicted half-life of 67 years.[9] Furthermore, if the half-lifetime of biochar is extrapolated to more than 1000 years,[14,15] polyaromatic carbons might not be the only determinant for the stabilities of biochars.

Apart from polyaromatic carbons, silica in biomass primarily consists of amorphous phytoliths and opal A particles.[16] For example, 80−98 wt % rice hull ash silicas are amorphous,[17] and they are always involved in the organic matrix mixture, forming a rigid microstructure that stabilizes the structures of plants[18] and presumably is bound to carbohydrates.[19] Silica ash can change the physical and structural compositions of biochar through pyrolysis via fusion and sintering.[3,13,20] As previously reported, lower ash contents and higher temperatures will produce more highly aromatic biochars.[11,21,22] Conversely, high ash contents may hinder the formation of aromatic carbon,[21] because minerals in the precursor samples act as a barrier to the diffusion of heat and the release of degraded volatiles during the charring process.[11] In addition, the fixed carbon contents were shown to decrease with increasing pyrolysis temperatures when biochars contained greater than 20% ash, suggesting possible interactions between organic and inorganic constituents during feedstock pyrolysis.[21] Furthermore, the presence of significant amounts of minerals may cause defects in aromatic structures, thereby reducing the number of cross-links between layers and decreasing the overall stability of a structure that is dominated by C links.[22] A wide distribution of silicon in the dry weight of biomass,[23] ranging from 0.1% to 10%,[24] generally causes silicon to accumulate in biochar during charring processes. With

Received: December 18, 2013
Revised: July 12, 2014
Accepted: July 14, 2014
Published: July 14, 2014

   dx.doi.org/10.1021/es405647e | Environ. Sci. Technol. 2014, 48, 9103−9112

increasing pyrolysis temperatures, the morphologies of the silicon components change from amorphous to crystalline,[13,25−27] resulting in interactions between silicon and carbon.[13] For example, a tiny amount of carbon from incompletely burned rice husk residue was not completely eliminated by higher and longer temperature treatments due to intertwined hydrated silica and lignocellulose.[27] Silicon may play an important role in arranging the heterogeneous structural composition of carbon pools,[13] including aromatic carbons, thereby having a considerable impact on carbon evolution when amended in soils. However, the roles of silicon components on the stabilities of biochars remain unknown.

Thus, identifying the mechanisms for the recalcitrance of biochars and elucidating the interactive effects of silicon and carbon components are critical for determining the stabilities of biochars, which is the primary objective of this study. The relative stabilities of biochars were examined via their carbon loss through chemical oxidation. Acidic hydrogen peroxide was employed to evaluate the stabilities of heterogeneous carbon pools because H_2O_2 as an oxidizer can remove >95% of natural organic matter[28] and decompose most refractory organic matter, especially aromatic carbons.[29,30] Therefore, this compound might be a promising indicator for distinguishing the heterogeneity of the labile and stable components of biochar. Short-term (24 h) and long-term (240 h) oxidation kinetics experiments with a series of H_2O_2 concentrations were conducted to evaluate carbon stability in rice-straw-derived biochars. The impacts of the preparation temperature and particle size on the carbon loss of biochars were examined. The microstructures of the raw biochars and oxidized biochars were characterized using scanning electron microscopy with energy dispersive spectrometry (SEM-EDS) and Fourier transform infrared spectroscopy (FTIR).

MATERIALS AND METHODS

Preparation of Biochars. Rice straw, one of the most abundant crop residues,[31] was collected from Anhui Province, China, and air-dried and milled through 30, 60, 100, and 200 mesh sieves. Five different particle sizes (<30, 30−60, 60−100, 100−200, and >200 mesh) of rice straw were prepared as the biomass precursors. Biochar was produced by pyrolyzing the biomasses under oxygen-limiting conditions at 300, 500, and 700 °C using a previously reported method.[6,7] Briefly, approximately 110 g of powdered rice straw was packed tightly in a ceramic crucible, which was then covered with a tight-fitting lid and then pyrolyzed in a muffle furnace for 4 h. The charred samples were sieved through 30, 60, 100, and 200 mesh sieves to obtain the final biochar samples. Biochars for RS300 with different particle sizes were named RS300-(<)30, RS300-30−60, RS300-60−100, RS300-100−200, and RS300-(>)200. The symbol of (<)30 corresponds to the particle size without being sieved through a 30 mesh sieve, thus the particle size of (<)30 is larger than that of 30−60, 60−100, 100−200, and >200. The symbol of (>)200 corresponds to the particles sieved through a 200 mesh sieve, which is less that the particle size of 30−60, 60−100, and 100−200. The other particle sizes lie within the different meshes. For example, RS300−30−60 means RS300 with the particle passed through 30 mesh sieve but intercepted by 60 mesh sieve. The RS500 and RS700 samples were characterized using the same procedures. RS300, RS500, and RS700 refer to rice straw biochars produced at 300, 500, and 700 °C, respectively.

Chemical Oxidation Kinetics Experiment. The chemical oxidation of biochars by H_2O_2 is commonly used to evaluate their recalcitrance, which is relevant to the degradation of biochar under natural soil conditions.[21,32−34] The concentration gradient of H_2O_2 in the oxidation experiments was regarded as the level of oxidation. Additionally, the stock concentration of H_2O_2 used in this study was 30% w/w, and it was diluted to different concentrations. The H_2O_2 oxidation experiment was conducted in a thermostatic water bath on the basis of a modification of a previously reported method.[28] The oxidation of organic matter by hydrogen peroxide is influenced by many parameters (such as temperature, pH, and concentration), with temperature being a key parameter: a higher temperature can accelerate the reaction rate and shorten the process. Because hydrogen peroxide rapidly decomposes at temperatures greater than 70 °C,[32] a suitable temperature of 60 °C was selected for the incubation experiment. Briefly, after 100 mg of biochar was added to a 50 mL plastic tube, 40.0 mL of H_2O_2 was slowly added to the tube and stirred with a vortex mixer for 1 min to ensure that the water and solid mixed well. The covered tube was placed in a thermostatic water bath, and the temperature was maintained at 60 ± 0.5 °C for 24 h for each treatment. During oxidation, the tube was repeatedly uncovered to release the air; the liquid was removed by filtration with a 0.45 μm membrane as soon as the experiment finished. The final oxidized residues were washed with deionized water and dried in an oven at 80 °C.

The following three oxidation kinetics experiments were performed: short-term (24 h) oxidation, long-term (240 h) oxidation and effect of particle size. (1) For short-term oxidation, 16 concentrations of H_2O_2 (0.0%, 0.5%, 1.0%, 2.0%, 3.0%, 4.0%, 6.0%, 8.0%, 10.0%, 12.0%, 15.0%, 18.0%, 21.0%, 24.0%, 27.0% and 30.0% w/w) were selected to investigate carbon stability in biochars under different levels of oxidation. The selected samples of RS300, RS500, and RS700 with 60−100 mesh particle sizes were reacted with H_2O_2 solutions in a one-time 24 h treatment. (2) For long-term oxidation, three H_2O_2 concentrations (0.5%, 2.0%, and 8.0%) were selected as the different oxidation levels, and RS300, RS500, and RS700 samples with 60−100 mesh particle sizes were selected as the model biochars. The long-term experiments consisted of 10 successive 24 h treatments to probe the microstructures and chemical characteristics of the multilayered composition of biochar. (3) To investigate the effect of particle size on carbon loss under different degrees of oxidation, five particle size ranges (<30, 30−60, 60−100, 100−200, and >200 mesh) of RS300, RS500, and RS700 and three concentrations of H_2O_2 (0.5%, 2.0%, and 8.0%) were selected for the 240 h oxidation treatments.

The carbon loss obtained from oxidation is defined as a negative increase from 0 to −100%. The carbon loss was calculated as follows:

$$C_{loss} = \frac{C_2 - C_1}{C_1} \times 100\% \quad (1)$$

Where C_{loss} represents the carbon loss percentage, C_1 refers to the carbon content in primary biochars, and C_2 refers to the carbon content in oxidized biochar residues.

Sample Characterization. The carbon contents (OC%) in the biochars and oxidized biochars were determined using a TOC-V carbon analysis instrument (SSM-5000A, Shimadzu, Japan). The ash contents (ash%) were measured by heating the

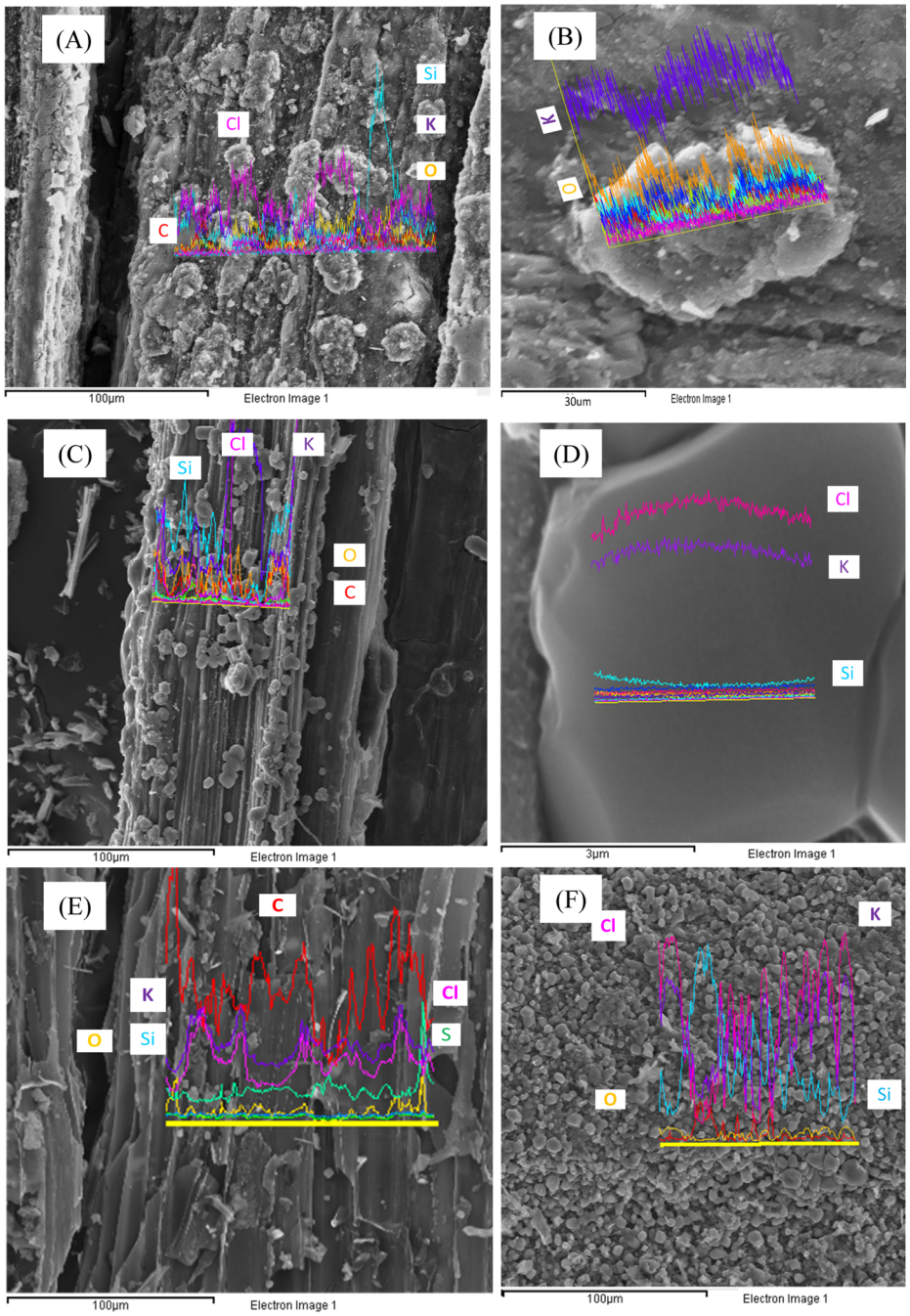

Figure 1. SEM-EDS images of RS300 (A, B), RS500 (C, D) and RS700 (E, F). (B) One spot of agglomeration in RS300 that mainly consisted of K_2O. (D) One of the crystals of potassium chlorite on the surface of RS500. (F) Shows the other surface of RS700 with accumulated silicate crystals. Note that the elemental components are the same color as the corresponding lines of the elements.

samples at 800 °C under an air atmosphere for 4 h. The organic carbon contents on an ash-free basis ($OC_{ash\text{-}free}$%) were calculated as $OC_{ash\text{-}free}$% = OC% / (100% − ash%). FTIR spectra were recorded in the 4000−400 cm^{-1} region with a resolution of 4 cm^{-1} using an FTIR spectrometer (Nicolet 6700, Thermo Scientific) and processed using the Thermo Scientific OMNIC software. SEM-EDS images of the samples were obtained by scanning the sample surfaces with a field-emission scanning electron microscopy (Quanta 3D FEG, FEI). EDS line spectra were acquired by drawing ∼60 μm arrows at a 1000× magnification for 300 s to achieve a sufficient signal-to-noise ratio. The results were autocorrected and optimized using the Inca software. The specific surface areas of the prepared biochars were measured by N_2 (0.162 nm^2) gas adsorption at liquid N_2 temperature (−196 °C) using a NOVA-2000E surface area analyzer. Prior to the surface area measurements, the samples were degassed under vacuum (less than 0.1 Pa) for 12 h at 378 K. Four data points, between relative pressures of 0.05 and 0.3, were used to determine the monolayer adsorption capacity.

RESULTS AND DISCUSSION

Characterization of the Rice-Straw-Derived Biochars. The carbon and ash contents in the RS300, RS500, and RS700 samples with different particle sizes are listed in Table S-1 of

dx.doi.org/10.1021/es405647e | Environ. Sci. Technol. 2014, 48, 9103−9112

the Supporting Information. For all of the biochar samples, the carbon content on an ash-free basis decreased with decreasing particle size, and the ash content correspondingly increased. According to the elemental compositions presented in Table S-2, RS700 was highly carbonized with polyaromatic carbon according to the measured O/C_{org} = 0.40 and H/C_{org} = 0.29. Comparatively, RS300 was the least carbonized biochar, with an elemental composition of O/C_{org} = 0.39 and H/C_{org} = 0.75, and RS500 had a considerably lower O/C_{org} = 0.33 but an intermediate H/C_{org} = 0.37, indicating that this sample was partially carbonized; these results are consistent with the previously reported NMR results[33] and with the standards of the International Biochar Initiative, as H/C_{org} <0.7 corresponds to a greater proportion of fused aromatic ring structures.[35] A large increase in aromaticity and a low degree of average condensation for biochars under 350−500 °C were observed, whereas average aromatic cluster sizes of 7−14 were observed for biochars at 500 °C ∼ 700 °C.[33] Only one particle size of 60−100 mesh was selected as a representative for the biochar structural characterization because biochars with this particle size were selected in most of the chemical oxidation experiments. The surface areas (SAs) of RS300 and RS500 were 18.54 and 11.75 m^2/g, respectively, which were smaller than the SA of RS700 (193.52 m^2/g), suggesting that the pores in RS700 were opened under the high carbonizing temperature.[7]

The SEM images and EDS line spectra of RS300, RS500 and RS700 are shown in Figure 1. As shown in Figure 1A,B, there were considerable amounts of KCl and K_2O on the surface of RS300. However, K_2O was not observed on the high-temperature biochars, which was consistent with a previous finding that K_2O was dissociated at 620 K to catalyze the melting of silica.[36] Interestingly, RS500 has a structure that contains silicon and carbon, which are possibly intertwined with each other but heterogeneously distributed (Figure 1C). We observed that KCl crystals were present on the surface of RS500 (Figure 1D). However, when the pyrolysis temperature increased to 700 °C, the KCl and silica became a mixture of aggregated crystallites that appeared on the opposite side of RS700 (Figure 1F), indicating that most of the silicon in the RS700 separated from the carbon structure (Figure 1E). Recently, Xiao et al.[13] systematically elucidated the transformation and morphology of carbon and silicon in rice straw biochars by XRD, FTIR, and SEM, and they found that increasing the pyrolysis temperature changed the silicon speciation from amorphous to crystalline, whereas the organic matter evolved from aliphatic to aromatic. A proposed mutual protection relationship[13] between carbon and silicon under different pyrolysis temperatures was used to explain the stability of carbon in RS500.

The FTIR spectra of RS300, RS500, and RS700 are shown in Figure S-1. The FTIR band assignments of biochars have been frequently described in previous reports.[6,7] In RS300, there were strong C═O stretching vibrations at 1704 cm^{-1},[6] C═O stretching vibrations of ketones at 1442 cm^{-1},[37] and C−O bending vibrations of phenols at 1380 cm^{-1},[38] but the relative intensities of these features decreased in RS500 and even disappeared in RS700, indicating increasing carbonization by the removal of O. The relative intensities of the C═C stretching vibrations at 1580−1619 cm^{-1} progressively declined from RS300 to RS700,[37,39] but there was a relatively broad peak located between 1569 and 1619 cm^{-1} for RS700, indicating the formation of different types of aromatic carbon forms compared with RS300 and RS500.

The peaks at 1100, 796, and 467 cm^{-1} were primarily assigned to Si−O−Si asymmetric vibrations, symmetrical stretching vibrations, and flexural vibrations, respectively.[38] As previously reported, the C−O stretching vibration also appeared in the range of 1170−950 cm^{-1}.[13] Biochars prepared at 300 °C are generally composed of residues of biopolymers such as cellulose,[6,7,40] so the possibility of C−O stretching cannot be excluded in RS300. The Si−O−Si peak at 1100−1050 cm^{-1} was mainly assigned to the stretching of Si−O,[41] which shifted from 1099 cm^{-1} for RS300 to 1091 cm^{-1} for RS500 and to 1056 cm^{-1} for RS700, indicating that the morphologies of silicon changed with increasing pyrolysis temperature. These results are supported by the SEM-EDS images shown in Figure 1.

Effect of Short-Term H_2O_2 Oxidation on the Carbon Losses of Biochars. Biochars prepared at three different temperatures (i.e., RS300, RS500 and RS700) exhibited different carbon loss trends under different concentrations of H_2O_2 during short-term oxidation (Figure 2). RS300 exhibited

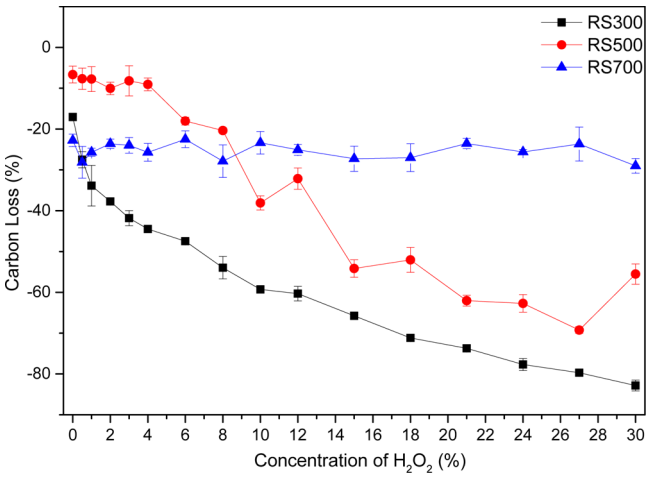

Figure 2. Carbon losses of RS300, RS500, and RS700 after short-term oxidation under 16 concentrations of H_2O_2 ranging from 0 to 30% with a particle size of 60−100 mesh.

an exponential-like loss of its carbon from −(17.1 ± 0.44)% to −(82.8 ± 1.33)%, whereas RS500 experienced three losses: a constant carbon loss of approximately −(8.2 ± 2.4)%, an increase from −18% to −54.2% and another constant loss with an average of −(62.8 ± 1.7)%. Therefore, the carbon pool of RS500 presumably consists of at least three components, including approximately 8.2% labile carbon (i.e., the initial decomposed carbon), 18−54% semilabile carbon, and 38−45% stable carbon. In contrast, RS700 maintained a constant carbon loss with an average of −(25.3 ± 2.3)% under different oxidation levels; this loss presumably consisted of easily removed labile carbon. RS700 is hypothesized to consist of two different pools corresponding to approximately 25% labile carbon and 75% stable carbon. The degree of oxidation barely influenced the carbon loss of RS700 in the short term.

When the H_2O_2 concentration was less than 8%, the carbon loss followed the sequence RS500 < RS700 < RS300, indicating that RS500 was more stable than the other two biochars under relatively low oxidation intensities. When the concentration of H_2O_2 increased to 8%, the carbon loss followed the sequence

dx.doi.org/10.1021/es405647e | Environ. Sci. Technol. 2014, 48, 9103−9112

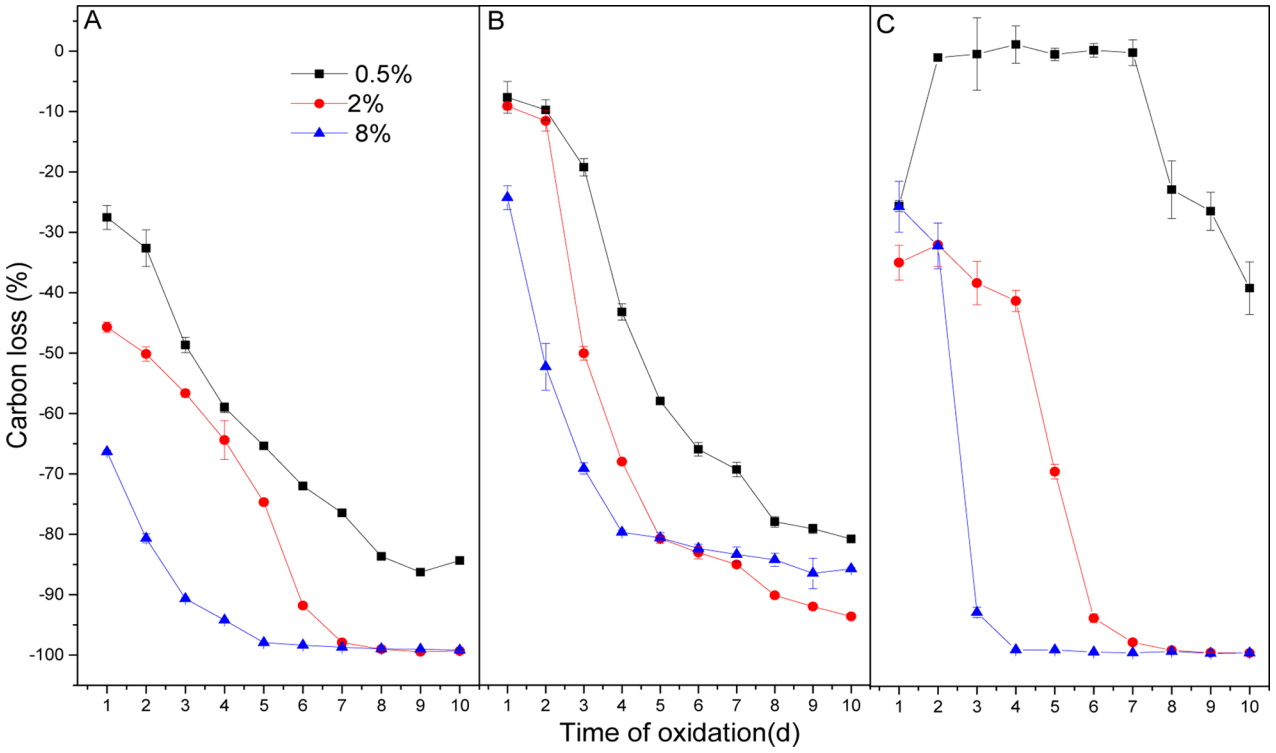

Figure 3. Carbon losses of RS300 (A), RS500 (B), and RS700 (C) with long-term oxidation under 0.5%, 2%, and 8% H_2O_2.

RS700 < RS500 <RS300, suggesting that RS700 was more stable than RS500 and RS300 under a higher degree of oxidation in the short term. These observations suggest that short-term oxidation clearly reveals the distinct carbon compositions of biochars and their different stabilities. Their recalcitrance mechanisms will be elucidated next.

Effect of Time-Dependent H_2O_2 Oxidation on the Carbon Losses of Biochars. The evolution of the carbon losses of RS300, RS500, and RS700 during 10 cycles of 24 h oxidation under 0.5%, 2%, and 8% H_2O_2 is shown in Figure 3. Because oxidation starts from the outer surface of the biochar,[42] each cycle of H_2O_2 oxidation in our experiment is regarded as the removal of one layer of carbon from the biochar. The degree of carbon removal was closely associated with the biochar preparation temperature and oxidation level. Under 0.5% H_2O_2, the carbon loss of RS300 was −27.5% for the first 24 h, which gradually increased with subsequent oxidation cycles up to −84.3% for the 10th 24 h oxidation cycle (Figure 3A). Under a higher degree of oxidation, the carbon loss of RS300 was enhanced, that is, from −45.7% for the first cycle to greater than −99.4% for the eighth cycle with 2% H_2O_2 and correspondingly from 66.3% to greater than −99.20% in the fifth cycle with 8% H_2O_2. These results suggest that there are no significant differences between the carbon structures from the external surfaces to the interiors of the RS300 particles, which cannot be distinguished by the degree of oxidation.

Compared with RS300, RS500 had smaller losses of −7.7% and −9.1% carbon under 0.5% and 2% H_2O_2, respectively, for the first oxidation cycle (Figure 3B). Even under 8% H_2O_2, no greater carbon loss was observed: the loss was only −24.5% compared with −66.3% for RS300. For RS500, there was a carbon loss of −80.8% after the 10th oxidation cycle under 0.5% H_2O_2. After the fifth cycle, the same carbon loss of approximately 80% occurred under 2% and 8% H_2O_2. Interestingly, the degree of oxidation insignificantly influenced the carbon losses of RS500, even at the high degrees of oxidation, because carbon losses of −93.6% under 2% H_2O_2 and −85.7% under 8% H_2O_2 were obtained after the 10th oxidation cycle. This result suggests that RS500 might consist of various carbon forms, in which at least 6.3% of the carbon is highly oxidation resistant and is encapsulated by silica, thereby protecting carbon from oxidation.

RS700 had a −25.6% carbon loss after the first 24 h oxidation cycle under 0.5% H_2O_2 (Figure 3C); thereafter, no further losses of carbon were observed until the seventh cycle. Interestingly, a sudden decrease in the carbon loss of −22.9% after the eighth cycle, followed by further continuous increases to −26.5% and −39.6% after the ninth and tenth oxidation cycles, respectively, were observed. RS700 exhibited a sharp carbon loss from initial values of −25.7% and −34.9% to similar carbon losses of −99.5% in the eighth and fourth oxidation cycles under 2% and 8% H_2O_2, respectively. These findings suggest that RS700 was primarily composed of two carbon pools (i.e., labile and stable carbon), which was defined as the fast- and slow-decomposed carbon pools,[43] respectively. The stable C pools mostly consist of highly aromatic and condensed C forms. Correspondingly, the fast carbon pool in RS700 accounted for approximately 25%, and the remainder belonged to the slow carbon pool. Again, among the tested biochars, RS500 possessed carbon that was highly oxidation resistant under long-term oxidation cycles, whereas RS300 had a comparatively homogeneous carbon pool under H_2O_2 oxidation regardless of the oxidation time or level.

Influence of Particle Sizes on the Carbon Losses of Biochar under Long-Term Oxidation Using H_2O_2. The carbon losses of RS300, RS500, and RS700 with five particle sizes after long-term oxidation with H_2O_2 are shown in Figure S-2. For 0.5% H_2O_2 (lower relative oxidation intensity), the three biochars generally showed similar trends (i.e., the largest particles had the lowest carbon losses). For 2% H_2O_2, this trend

dx.doi.org/10.1021/es405647e | Environ. Sci. Technol. 2014, 48, 9103−9112

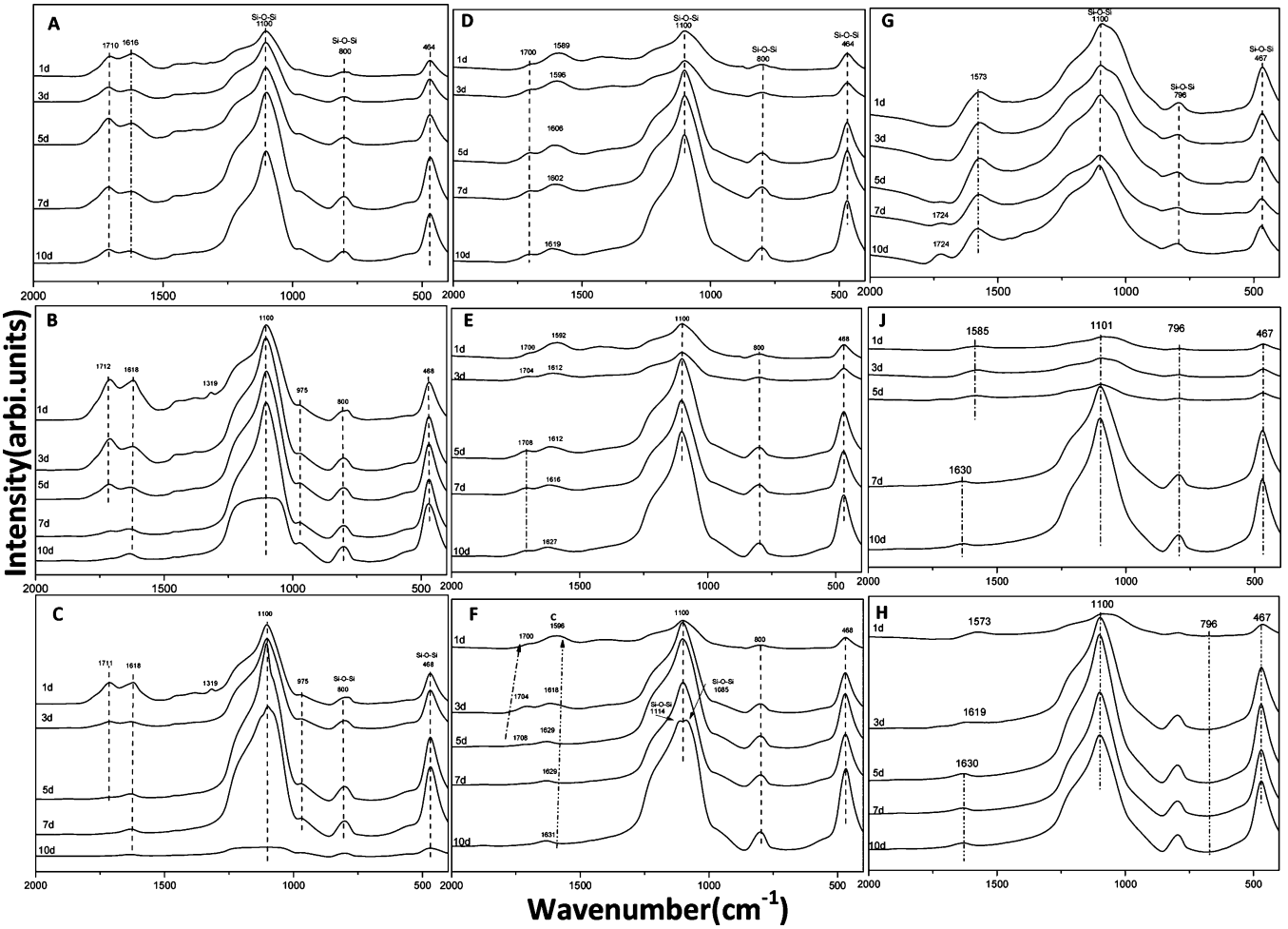

Figure 4. Stacked FTIR spectra of RS300 (A, B, C), RS500 (D, E, F) and RS700 (G, J, H) after long-term oxidation, in which were tested the following conditions: A, D, G were tested under 0.5% H_2O_2; B, F, J were under tested under 2% H_2O_2; and C, F, H were tested under 8% H_2O_2.

was less significant, and for 8% H_2O_2, no observable differences among particles could be found, which is consistent with the FTIR results shown in Figure S-3 and with the detailed information presented in Supporting Information, indicating that large particles affected the mineralization rate of biochar.[44] Two mechanisms have been proposed to explain these phenomena. ~~First~~, large particles contain more aromatic regions and fewer reactive sites upon hydrolysis and oxidation compared with smaller particles because the larger particles have more distinct heterogeneous components than the smaller ones.[20] ~~Second~~, the environmental degradation of the biochar represent surface photo-oxidation and chemical-oxidation phenomena;[20,45] therefore, larger particles would oxidize more slowly and presumably have a longer turnover time than smaller particles. In contrast, Nguyen et al. found that a large amount of large particles were broken into smaller particles of <5 μm after 30 years,[46] whereas the smaller <5 μm particles became considerably more stable when adsorbed to soil minerals,[47] with a longer turnover time of greater than 100 years. Our results suggest that the smaller particles generally experience greater oxidation because they have a larger surface area compared to the larger particles, and therefore, they potentially have a more reactive surface. Therefore, it can be concluded that large particles may potentially play a determining role in the initial degradation of biochar in soil.

FTIR Spectra of Oxidized Biochars. The FTIR spectra of oxidized RS300, RS500, and RS700 after five different oxidation cycles under 0.5%, 2%, and 8% H_2O_2 are shown in Figure 4. For RS300, the stretching vibrations of C═C at 1616 cm^{-1} and C═O at 1710 cm^{-1} initially increased but then rapidly decreased in later oxidation cycles. Under 0.5% H_2O_2, the Si−O−Si peaks at 1100, 800, and 464 cm^{-1} continuously increased, and simultaneously, changes in the C═C and C═O peaks occurred. Higher degrees of oxidation led to a rapid decrease in the C═C and C═O peaks and finally removed the C═O peak, followed by the C═C peak, whereas the Si−O−Si peak initially increased and then rapidly decreased, and this peak almost completely disappeared (Figure 4B,C). These phenomena were more significant under 8% H_2O_2, indicating that the carbon loss in RS300 is minimally affected by silicon components but strongly affected by the degree of oxidation. Therefore, these results may explain why the carbon components in RS300 cannot be distinguished under oxidation with H_2O_2.

For RS500 (Figure 4D−F), the evolution of the FTIR spectra with subsequent oxidation cycles was quite different from that for RS300. Under 0.5% H_2O_2, the C═O peaks were located at 1700 cm^{-1}, and the C═C peaks shifted from 1589 to 1619 cm^{-1} with subsequent oxidation cycles, but their peak intensities remained almost unchanged. Correspondingly, the intensities of the Si−O−Si peaks at 1100, 800, and 464 cm^{-1}

dx.doi.org/10.1021/es405647e | Environ. Sci. Technol. 2014, 48, 9103−9112

gradually increased, indicating that removal of carbon made vibrations of the remaining "naked Si−O−Si bond" considerably stronger. Higher oxidation resulted in slight but gradual decreases in the intensities of the C═C and C═O peaks and even removed the C═O peak. In contrast, the Si−O−Si peak intensities increased with increasing oxidation cycles, and the peak at 1100 cm^{-1} split into two peaks (i.e., 1114 and 1085 cm^{-1}, Figure 4F) after the 10th oxidation cycle, which indicated that two types of silica components were present in RS500. The evolution of the FTIR spectra assigned to the carbon and silicon components strongly suggests that carbon is closely associated with silicon and that the presence of silicon has a significant impact on the carbon losses of RS500 under all of the aforementioned oxidation conditions. The high degree of oxidation has a less significant influence on the carbon loss, especially during the later stages of oxidation.

However, RS700 exhibited completely different FTIR spectral changes under the three oxidation conditions (Figures 4G, J, H). Under 0.5% H_2O_2, there were stronger C═C stretching vibrations at 1573 cm^{-1}, and no significant changes were observed for the oxidized biochars. A C═O peak appeared at 1724 cm^{-1} after the seventh oxidation cycle, indicating that the initial oxidation had no observable effect on the carbon structure and that the surface oxidation of RS700 was progressive. The Si−O−Si peak intensities remained unchanged, but the Si−O peaks at 1052 cm^{-1} gradually disappeared, which indicated that part of the silica was easily removed. For RS700 under 2% and 8% H_2O_2, the C═O peaks disappeared, the C═C peaks dramatically decreased, and only small peaks remained after the first oxidation cycle. Correspondingly, the intensities of the Si−O−Si peaks became considerably stronger with increasing oxidation cycles. The Si−O peak at 1052 cm^{-1} was removed faster under higher degrees of oxidation. This peak disappeared after the third oxidation cycle under 2% H_2O_2, and it disappeared after the first oxidation cycle under 8% H_2O_2, suggesting that these forms of silicon were relatively easily removed by H_2O_2 oxidation. The carbon in RS700 could thus be concluded to consist mainly of polyaromatic carbon forms, with the isolated silica in RS700 having a less significant impact on the carbon loss.

The FTIR spectra of RS500 after the 10 day oxidation under 0.5%, 2%, and 8% with five different particle sizes are shown in Figure S-3. After 0.5% H_2O_2 oxidation, the intensities of the peaks of C═C at 1599−1628 cm^{-1} and of C═O at 1708 cm^{-1} increased with decreasing particle size. Conversely, the intensities of the Si−O−Si peaks decreased with increasing particle size, suggesting that the large particles contained less silicon than the small particles, which might partially explain why the larger particles exhibited higher antioxidation abilities. Higher oxidation under 2% and 8% H_2O_2 resulted in significant changes of all peaks, with stronger Si−O−Si peaks, weaker C═C and C═O peaks and even the removal of C═O peaks, as shown in Figure S-3B, S-3C. Thus, the high degree of oxidation had a more significant impact on the carbon loss than the particle size.

SEM Images of Oxidized RS500 and RS700. The SEM images of the oxidized biochars after the first, third, fifth and tenth cycles of 24 h oxidation under 2% H_2O_2 are shown in Figure 5 for RS500 and in Figure S-4 for RS700. The SEM images provided a clear map of the oxidized biochars and are in sharp contrast to the as-prepared biochars. After H_2O_2 oxidation, the solid structures of RS500 with smooth surfaces in Figure 5A were eroded into rough surfaces, and both large

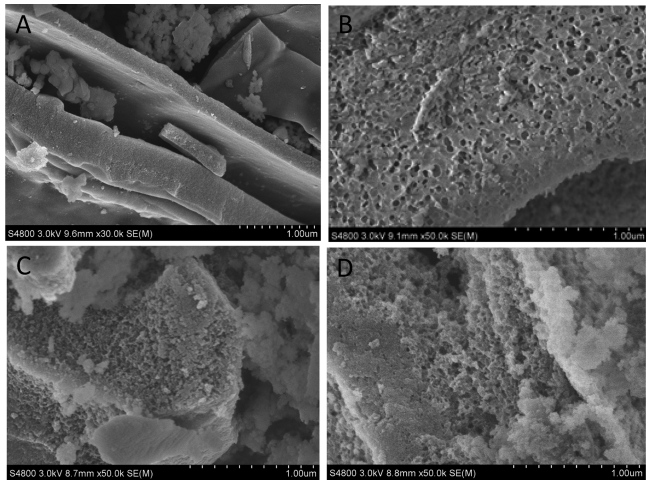

Figure 5. SEM images of RS500 after the first (A), third (B), fifth (C) and tenth (D) successive 24 h treatment under 2% H_2O_2.

and small concave pits with diameters ranging from approximately 100 to 615 nm are observed in Figure 5B. This erosive effect became greater with further oxidation. More concave regions appeared, and the smaller pits were filled. In addition, the oxidized structure became considerably looser, but a relatively clear structure still remained, as shown in Figure 5C,D. This observation indicated the preservation of carbon in RS500, which was supported by the aforementioned results that 14.3% carbon remained after oxidation and by the FTIR spectra in Figure 5D−F. Furthermore, upon surface oxidation, the repeated oxidation could result in a sequential multilayer removal of carbon in the outside layer while the carbon inside could survive. Therefore, a sufficient degree of oxidation could completely decompose any form of carbon, but the encapsulated carbon would be unaffected and survive.

RS700 was initially covered with ash components (Figure S-4A). Further oxidation exposed a clear intact and dense structure (Figure S-4B). After the fifth oxidation cycle, the biochar residues exhibited more distinct features with more large and small holes, indicating that the biochar structures were partially destroyed. As shown in Figure S-4D, after the 10th oxidation cycle, no dense structure could be observed, but a large number of porous particles were observed, demonstrating that the entire structure had been almost completely destroyed, with nearly no carbon components surviving after strong oxidation. On the basis of the above SEM images, we determined that the structure of RS700 was considerably easier to break than that of RS500.

Recalcitrance Mechanism for the Stability of Rice-Straw-Derived Biochars. There have been no systematic investigations of the recalcitrance mechanism to explain the stabilities of biochars, although many studies have considered aromaticity to be a main contributor. As Lehmann proposed,[2] several factors that influence the recalcitrance of biochars hinder the precise prediction of their half-life in soils. Many other factors, such as strongly interlinked iron and organic carbon,[28] might affect the recalcitrance of organic carbon in a biochar.

Our investigation provided a new perspective regarding carbon forms and silicon morphologies and the effect of their coupled interaction on the stabilities of biochars. The tested biochars (RS300, RS500, and RS700) exhibited different stability mechanisms. Both the short-term and long-term

dx.doi.org/10.1021/es405647e | Environ. Sci. Technol. 2014, 48, 9103−9112

oxidation results indicated that the low-temperature biochar (RS300) was partially carbonized, which included non-carbonized and carbonized organic matter.[6] The noncarbonized organic matter was labile carbon, and the carbonized matter was also easily decomposed by an oxidizer such as H_2O_2. Carbon losses under long-term oxidation resulted in at least 6.3% of the carbon, including aromatic carbon, remaining in the oxidized residues of RS500. This finding is partially related to the fact that ash minerals change their physical and structural compositions during pyrolysis via fusion and sintering.[3,13] Notably, the varying morphologies of silicon components with increasing temperature, changing from amorphous to crystalline,[25−27] and silicon phase changes from metastable α-quartz to stable β-quartz[48,49] were presumed to be the main contributors to this intertwined structure and the encapsulation of carbon by silica.[36] Reasonably, the Si-encapsulated carbon is more physically stable than other forms of carbon components fixed by surface adsorption.

We determined that RS700 primarily consisted of 25% labile carbon and 75% highly stable carbon. The latter remained constant from the second to seventh 24 h oxidation cycle because RS700 had characteristics similar to that of basic activated carbon[43] and may act as a BC/BC$^+$ (BC refers to black carbon) electron-carrier catalyst similar to AC/AC$^+$ (AC refers to activated carbon).[50] The surface of RS700 catalyzed a certain moiety of radical (OH·) formation[50] and concurrently catalyzed the decomposition of H_2O_2 into O_2 and H_2O.[43] However, the sudden carbon loss in the eighth oxidation cycle denoted the start of structural destruction, which was due to the erosive effect of these radicals (OH·) and caused destruction of the biochar itself, as indicated by the increasing C═O peaks and decreasing C═C peaks in the FTIR spectra with enhanced oxidation. In general, the stability of carbon in RS700 is mainly attributed to highly polyaromatic carbon, which can catalyze the decomposition of H_2O_2 and prevent itself from being damaged for a considerable length of time; only a sufficient degree of oxidation could destroy its aromatic structure. Biochar might therefore lose its catalytic function, indicating that RS700 is presumably relatively stable under low oxidation levels in the soil, which could ensure the long turnover time of biochar.

To elucidate the recalcitrance mechanism for the carbon stability of biochars, we initially propose a framework model in Figure 6 for the silicon−carbon-coupling mechanism that affects the stability of biochars. Silicon is a key factor that influences the arrangement of carbon and its structural composition. RS300 biochar mainly consists of partly carbonized carbon[6,7] and amorphous silica.[13] For RS500, the silicon was blended with carbon and formed a dense structure,[13] forming Si-encapsulated carbon. However, for RS700, the silicon components were changed into the crystalline phase and separated from the carbon structure. They subsequently formed larger silica crystals and enlarged the naked polyaromatic carbon regions.[13] Thus, this polyaromatic carbon is the main contributor to the stability of RS700, which is consistent with the results from Ascough et al.,[51] who reported that aromatic compounds larger than 19-ring PAHs were abundant at ≥700 °C but that no fused rings > coronene (7 rings) were present at <500 °C. Note that KCl crystals were present in all temperature-dependent biochars (RS300, RS500 and RS700), but its distribution is closely related with silica and plays a role in catalyzing the melting of silica.[27,36]

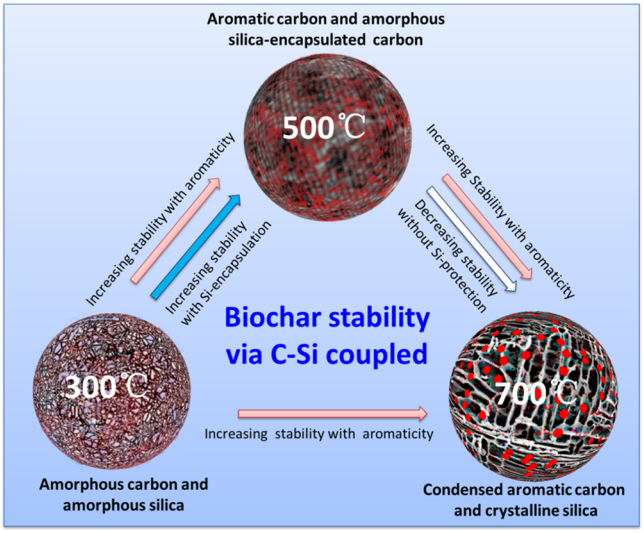

Figure 6. Model proposed for a silicon−carbon-coupling mechanism that affects the stability of biochar.

These investigations reveal that the stability of biochars is not only determined by aromatic structures but also influenced by silicon protection and particle size. The interaction between Si and C provides a new perspective for assessing the stability of biochar with respect to its soil carbon storage potential and fills a gap in understanding the stability associated with the morphologies of carbon and silica. This silica-encapsulated carbon structure can protect the biochar against physical and chemical oxidation and presumably leads to a longer turnover time in soils and thus a greater potential for carbon sequestration. More studies are required to probe the evolution of biochar turnover and associated lifetime related with silica as a whole and their molecular composition at nanoscale levels.

■ ASSOCIATED CONTENT

Ⓢ Supporting Information

The elemental compositions and ash contents of the biochars are presented in Table S-1 and S-2. The FTIR spectra of primary biochars are presented in Figure S-1. The carbon losses of RS300, RS500, and RS700 with five types of particle sizes after long-term oxidation are presented in Figure S-2. Stacked FTIR spectra of RS500 with different particle sizes are presented in Figure S-3. SEM images of RS700 after different oxidations are presented in Figure S-4. This material is available free of charge via the Internet at http://pubs.acs.org.

■ AUTHOR INFORMATION

Corresponding Author

*E-mail: blchen@zju.edu.cn. Fax: 0086-571-88982587. Tel.: 0086-571-88982587.

Notes

The authors declare no competing financial interest.

■ ACKNOWLEDGMENTS

This project was supported by the National Basic Research Program of China (Grants 2014CB441106), the National Natural Science Foundation of China (Grants 21277120, 41071210 and 20890111).

REFERENCES

(1) Laird, D. A. The charcoal vision: A win-win-win scenario for simultaneously producing bioenergy, permanently sequestering carbon, while improving soil and water quality. *Agron. J.* **2008**, *100* (1), 178−181.

(2) Lehmann, J. Bio-energy in the black. *Front. Ecol. Environ.* **2007**, *5* (7), 381−387.

(3) Lehmann, J.; Czimczik,C. I.; Laird, D.; Sohi, S. In *Biochar for Environmental Management. Science and Technology*; Lehmann, J., Joseph, S., Eds; Earthscan Publications: London, U.K., 2009; pp 183−205.

(4) Masiello, C. A. New directions in black carbon organic geochemistry. *Mar. Chem.* **2004**, *92* (1−4), 201−213.

(5) Hedges, J. I.; Eglinton, G.; Hatcher, P. G.; Kirchman, D. L.; Arnosti, C.; Derenne, S.; Evershed, R. P.; Kogel-Knabner, I.; de Leeuw, J. W.; Littke, R.; Michaelis, W.; Rullkotter, J. The molecularly-uncharacterized component of nonliving organic matter in natural environments. *Org. Geochem.* **2000**, *31* (10), 945−958.

(6) Chen, B.; Zhou, D.; Zhu, L. Transitional adsorption and partition of nonpolar and polar aromatic contaminants by biochars of pine needles with different pyrolytic temperatures. *Environ. Sci. Technol.* **2008**, *42* (14), 5137−5143.

(7) Chen, Z.; Chen, B.; Chiou, C. T. Fast and slow rates of naphthalene sorption to biochars produced at different temperatures. *Environ. Sci. Technol.* **2012**, *46* (20), 11104−11111.

(8) Keiluweit, M.; Nico, P. S.; Johnson, M. G.; Kleber, M. Dynamic molecular structure of plant biomass-derived black carbon (biochar). *Environ. Sci. Technol.* **2010**, *44* (4), 1247−1253.

(9) Zimmermann, M.; Bird, M. I.; Wurster, C.; Saiz, G.; Goodrick, I.; Barta, J.; Capek, P.; Santruckova, H.; Smernik, R. Rapid degradation of pyrogenic carbon. *Global Change Biol.* **2012**, *18* (11), 3306−3316.

(10) Zhao, L.; Cao, X.; Wang, Q.; Yang, F.; Xu, S. Mineral constituents profile of biochar derived from diversified waste biomasses: implications for agricultural applications. *J. Environ. Qual.* **2013**, *42* (2), 545−552.

(11) Xu, Y.; Chen, B. Investigation of thermodynamic parameters in the pyrolysis conversion of biomass and manure to biochars using thermogravimetric analysis. *Bioresour. Technol.* **2013**, *146*, 485−493.

(12) Simpson, M.; Hatcher, P. Overestimates of black carbon in soils and sediments. *Naturwissenschaften* **2004**, *91* (9), 436−440.

(13) Xiao, X.; Chen, B.; Zhu, L. Transformation, morphology and dissolution of silicon and carbon in rice straw derived biochars under different pyrolytic temperatures. *Environ. Sci. Technol.* **2014**, *48* (6), 3411−3419.

(14) Preston, C. M.; Schmidt, M. W. I. Black (pyrogenic) carbon: A synthesis of current knowledge and uncertainties with special consideration of boreal regions. *Biogeosciences* **2006**, *3* (4), 397−420.

(15) Lehmann, J.; Skjemstad, J.; Sohi, S.; Carter, J.; Barson, M.; Falloon, P.; Coleman, K.; Woodbury, P.; Krull, E. Australian climate-carbon cycle feedback reduced by soil black carbon. *Nat. Geosci.* **2008**, *1* (12), 832−835.

(16) Desplanques, V.; Cary, L.; Mouret, J. C.; Trolard, F.; Bourrie, G.; Grauby, O.; Meunier, J. D. Silicon transfers in a rice field in Camargue (France). *J. Geochem. Explor.* **2006**, *88* (1−3), 190−193.

(17) Asuncion, M. Z.; Hasegawa, I.; Kampf, J. W.; Laine, R. M. The selective dissolution of rice hull ash to form $[OSiO_{1.5}]_8[R_4N]_8$(R = Me, CH_2CH_2OH) octasilicates. Basic nanobuilding blocks and possible models of intermediates formed during biosilicification processes. *J. Mater. Chem.* **2005**, *15* (21), 2114−2121.

(18) Datnoff, L. E.; Rodrigues, F. A. Silicon and rice disease management. *Fitopatologia Brasiliera* **2005**, *30* (5), 457−469.

(19) Freitas, J. C. C.; Emmerich, F. G.; Bonagamba, T. J. High-resolution solid-state NMR study of the occurrence and thermal transformations of silicon-containing species in biomass materials. *Chem. Mater.* **2000**, *12* (3), 711−718.

(20) Rumpel, C.; Gonzalez-Perez, J. A.; Bardoux, G.; Largeau, C.; Gonzalez-Vila, F. J.; Valentin, C. Composition and reactivity of morphologically distinct charred materials left after slash-and-burn practices in agricultural tropical soils. *Org. Geochem.* **2007**, *38* (6), 911−920.

(21) Enders, A.; Hanley, K.; Whitman, T.; Joseph, S.; Lehmann, J. Characterization of biochars to evaluate recalcitrance and agronomic performance. *Bioresour. Technol.* **2012**, *114*, 644−653.

(22) Nguyen, B. T.; Lehmann, J. Black carbon decomposition under varying water regimes. *Org. Geochem.* **2009**, *40* (8), 846−853.

(23) Epstein, E. Silicon: its manifold roles in plants. *Ann. Appl. Biol.* **2009**, *155* (2), 155−160.

(24) Ma, J. F.; Takahashi, E. *Soil, Fertilizer, and Plant Silicon Research in Japan*; Elsevier Science: Amsterdam, 2002.

(25) Mochidzuki, K.; Sakoda, A.; Suzuki, M.; Izumi, J.; Tomonaga, N. Structural behavior of rice husk silica in pressurized hot-water treatment processes. *Ind. Eng. Chem. Res.* **2001**, *40* (24), 5705−5709.

(26) Thy, P.; Jenkins, B. M.; Grundvig, S.; Shiraki, R.; Lesher, C. E. High temperature elemental losses and mineralogical changes in common biomass ashes. *Fuel* **2006**, *85* (5−6), 783−795.

(27) Wang, W. X.; Martin, J. C.; Zhang, N.; Ma, C.; Han, A. J.; Sun, L. Y. Harvesting silica nanoparticles from rice husks. *J. Nanopart. Res.* **2011**, *13* (12), 6981−6990.

(28) Lalonde, K.; Mucci, A.; Ouellet, A.; Gelinas, Y. Preservation of organic matter in sediments promoted by iron. *Nature* **2012**, *483* (7388), 198−200.

(29) Kumar, S. M. Degradation and mineralization, of organic contaminants by Fenton and photo-Fenton processes: Review of mechanisms and effects of organic and inorganic additives. *Res. J. Chem. Environ.* **2011**, *15* (2), 96−112.

(30) Heard, I.; Senftle, F. E. Chemical oxidation of anthracite with hydrogen-peroxide via the Fenton reaction. *Fuel* **1984**, *63* (2), 221−226.

(31) Kim, S.; Dale, B. E. Global potential bioethanol production from wasted crops and crop residues. *Biomass Bioenergy* **2004**, *26* (4), 361−375.

(32) Gray, A. B.; Pasternack, G. B.; Watson, E. B. Hydrogen peroxide treatment effects on the particle size distribution of alluvial and marsh sediments. *Holocene* **2010**, *20* (2), 293−301.

(33) McBeath, A. V.; Smernik, R. J.; Schneider, M. P. W.; Schmidt, M. W. I.; Plant, E. L. Determination of the aromaticity and the degree of aromatic condensation of a thermosequence of wood charcoal using NMR. *Org. Geochem.* **2011**, *42* (10), 1194−1202.

(34) Knicker, H.; Gonzalez-Vila, F. J.; Gonzalez-Vazquez, R. Biodegradability of organic matter in fire-affected mineral soils of Southern Spain. *Soil Biol. Biochem.* **2013**, *56*, 31−39.

(35) International Biochar Initiative (IBI). Appendix 5—The use of $H:C_{org}$ to indicate C stability. In version 1.1 of the *IBI Biochar Standards* to address technical program revisions; IBI: Westerville, OH,2013; pp 33−35. http://www.biochar-international.org/characterizationstandard.

(36) Krishnarao, R. V.; Subrahmanyam, J.; Kumar, T. J. Studies on the formation of black particles in rice husk silica ash. *J. Eur. Ceram. Soc.* **2001**, *21* (1), 99−104.

(37) Kloss, S.; Zehetner, F.; Dellantonio, A.; Hamid, R.; Ottner, F.; Liedtke, V.; Schwanninger, M.; Gerzabek, M. H.; Soja, G. Characterization of slow pyrolysis biochars: effects of feedstocks and pyrolysis temperature on biochar properties. *J. Environ. Qual.* **2012**, *41* (4), 990−1000.

(38) Liu, P.; Liu, W.; Jiang, H.; Chen, J.; Li, W.; Yu, H. Modification of bio-char derived from fast pyrolysis of biomass and its application in removal of tetracycline from aqueous solution. *Bioresour. Technol.* **2012**, *121*, 235−240.

(39) Aydincak, K.; Yumak, T.; Sinag, A.; Esen, B. Synthesis and characterization of carbonaceous materials from saccharides (glucose and lactose) and two waste biomasses by hydrothermal carbonization. *Ind. Eng. Chem. Res.* **2012**, *51* (26), 9145−9152.

(40) Lehmann, J.; Solomon, D. Organic carbon chemistry in soils observed by synchrotron-based spectroscopy. *Dev. Soil Sci.* **2010**, *34*, 289−312.

(41) Sarangi, M.; Nayak, P.; Tiwari, T. N. Effect of temperature on nano-crystalline silica and carbon composites obtained from rice-husk ash. *Composites, Part B: Engineering* **2011**, *42* (7), 1994−1998.
(42) Lehmann, J.; Liang, B. Q.; Solomon, D.; Lerotic, M.; Luizao, F.; Kinyangi, J.; Schafer, T.; Wirick, S.; Jacobsen, C. Near-edge X-ray absorption fine structure (NEXAFS) spectroscopy for mapping nano-scale distribution of organic carbon forms in soil: Application to black carbon particles. *Global Biogeochem. Cycles* **2005**, *19* (1), 1−12.
(43) Khalil, L. B.; Girgis, B. S.; Tawfik, T. A. M. Decomposition of H_2O_2 on activated carbon obtained from olive stones. *J. Chem. Technol. Biotechnol.* **2001**, *76* (11), 1132−1140.
(44) Joseph, S. D.; Camps-Arbestain, M.; Lin, Y.; Munroe, P.; Chia, C. H.; Hook, J.; van Zwieten, L.; Kimber, S.; Cowie, A.; Singh, B. P.; Lehmann, J.; Foidl, N.; Smernik, R. J.; Amonette, J. E. An investigation into the reactions of biochar in soil. *Aust. J. Soil Res.* **2010**, *48* (6−7), 501−515.
(45) Brodowski, S.; Amelung, W.; Haumaier, L.; Abetz, C.; Zech, W. Morphological and chemical properties of black carbon in physical soil fractions as revealed by scanning electron microscopy and energy-dispersive X-ray spectroscopy. *Geoderma* **2005**, *128* (1−2), 116−129.
(46) Nguyen, B. T.; Lehmann, J.; Kinyangi, J.; Smernik, R.; Riha, S. J.; Engelhard, M. H. Long-term black carbon dynamics in cultivated soil. *Biogeochemistry* **2008**, *89* (3), 295−308.
(47) Krull, E. S.; Baldock, J. A.; Skjemstad, J. O. Importance of mechanisms and processes of the stabilisation of soil organic matter for modelling carbon turnover. *Funct. Plant Biol.* **2003**, *30* (2), 207−222.
(48) Lager, G. A.; Jorgensen, J. D.; Rotella, F. J. Crystal-structure and thermal-expansion of alpha-quartz Sio2 at low-temperatures. *J. Appl. Phys.* **1982**, *53* (10), 6751−6756.
(49) Wiberg, E.; Wiberg, N. *Inorganic Chemistry*; Academic Press: San Diego, CA, 2001.
(50) Kimura, M.; Miyamoto, I. Discovery of the activated-carbon radical AC^+ and the novel oxidation-reactions comprising the AC/AC^+ cycle as a catalyst in an aqueous-solution. *Bull. Chem. Soc. Jpn.* **1994**, *67* (9), 2357−2360.
(51) Ascough, P. L.; Bird, M. I.; Meredith, W.; Wood, R. E.; Snape, C. E.; Brock, F.; Higham, T. F. G.; Large, D. J.; Apperley, D. C. Hydropyrolysis: implications for radiocarbon pretreatment and characterization of black carbon. *Radiocarbon* **2010**, *52* (3), 1336−1350.